

IMUSE: IMU-based Facial Expression Capture

Youjia Wang^{1,2*} Yiwen Wu^{1,2*} Hengan Zhou^{1,2} Hongyang Lin^{1,3} Xingyue Peng¹
Yingwenqi Jiang¹ Yingsheng Zhu¹ Guanpeng Long^{1,4} Yatu Zhang¹ Jingya Wang¹
Lan Xu¹ Jingyi Yu¹

¹ShanghaiTech University ²LumiAni Technology ³Deemos Technology ⁴ElanTech Co., Ltd.

{wangyj2, wuyw2023, zhouha, linhy, pengxy2023, jiangywq, zhuysh, longgp2022, zhangyt2023, wangjingya, xulan1, yujingyi}@shanghaitech.edu.cn

<https://sites.google.com/view/projectpage-imuse>



Figure 1. We introduce IMUSE, an innovative facial capture system based on IMUs. Using flexible electronic materials, we fabricate miniature IMUs that attach to the human face. Without relying on any visual signals, IMUSE can accurately reconstruct facial expressions.

Abstract

For facial motion capture and analysis, the dominated solutions are generally based on visual cues, which cannot protect privacy and are vulnerable to occlusions. Inertial measurement units (IMUs) serve as potential rescues yet are mainly adopted for full-body motion capture. In this paper, we propose IMUSE to fill the gap, a novel path for facial expression capture using purely IMU signals, significantly distant from previous visual solutions. The key design in our IMUSE is a trilogy. We first design micro-IMUs to suit facial capture, companion with an anatomy-driven IMU placement scheme. Then, we contribute a novel IMU-ARKit dataset, which provides rich paired IMU/visual sig-

nals for diverse facial expressions and performances. Such unique multi-modality brings huge potential for future directions like IMU-based facial behavior analysis. Moreover, utilizing IMU-ARKit, we introduce a strong baseline approach to accurately predict facial blendshape parameters from purely IMU signals. The IMUSE framework empowers us to perform accurate facial capture in scenarios where visual methods falter and simultaneously safeguard user privacy. We conduct extensive experiments about both the IMU configuration and technical components to validate the effectiveness of our IMUSE approach. Notably, IMUSE enables various potential and novel applications, i.e., facial capture against occlusions or in a moving performance. We will release our dataset and implementations

to enrich more possibilities of facial capture and analysis in our community.

1. Introduction

Latest successes in visual inference and generation are largely driven by a symbiotic relationship between advancements in algorithms and developments in sensor technology. Creative use of sensors beyond traditional RGB cameras has further inspired innovation across various domains. Most notably, Inertial Measurement Unit or IMUs, initially used in mobile devices, have been progressively embraced in whole-body motion capture. In comparison to conventional vision-based systems, IMUs boast portability and minimal spatial prerequisites. Typically attached to various body joints, IMUs can capture essential acceleration and axis angle data that can further translate to body motion. For example, pioneering work by Loper et al. [46] adapted this axis angle data for integration with the SMPL human body model, thereby enabling full-body motion capture. Most recently, Yi et al. [86] achieved comprehensive body motion capture using as few as six IMUs, leveraging the stability and generative capabilities of Transformer Diffusion [41].

In this paper, we explore using IMUs for facial expression capture. Facial expressions, as subtle as minute muscle movements, play a key role in effectively conveying a wide range of emotions as well as providing emotional depth beyond spoken words. By far capturing and analyzing facial expressions have predominantly depended on visual cues captured by RGB cameras. Techniques such as 3DDFA [30, 97] and DECA [26] offer a rapid means of acquiring facial geometry and expression from image or video streams. By employing RGBD cameras, Apple’s ARKit[5] supports real-time facial geometry acquisition for creating animated avatars that mimic human expressions. For visual-based techniques (RGB or RGBD) to work, cameras must have a clear line of sight to the subject’s face and the facial images need to be captured in adequate lighting. This is particularly problematic when the subject’s face is partially obstructed (e.g., during drinking or eating) or poorly lit (e.g., outdoors at night). In addition, having a person facing towards the camera all the time not only is infeasible but also significantly limits their body movements.

We hence present IMUSE, an IMU-based facial expression capture system that provides a camera-free alternative to current visual-based solutions. Existing IMUs for whole-body motion capture, however, are not readily deployable to faces. Hardware-wise, integrating IMUs with additional sensors (like inertial and geomagnetic detectors) and communication modules (such as Bluetooth and Wi-Fi) results in a size prohibitive large and uncomfortable for faces. Algorithm-wise, IMUs offer much sparser spatial signals than visual data and they intend to have much

lower signal-to-noise ratios. Furthermore, unlike body motion capture where spatial positions correlate to bone rotations, facial expressions are predominantly muscle-driven, posing a unique challenge in meaningfully translating IMU data.

To address these issues, IMUSE first tailors IMU designs to target facial applications, emphasizing miniaturization. Specifically, by separating the detection and data modules of the IMU, we ensure that the device attached to the face is compact and lightweight. For the detection module, we use a flexible material design to ensure that it adheres to the surface of the face, which ensures that the signal is captured accurately and is more comfortable for the user. This design avoids interfering with natural facial movements and allows reliable data transmission and synchronization.

IMUSE adopts an anatomy-driven strategy for placing IMUs in correspondence with specific muscles that control facial expressions. Using IMUSE, we collect the first facial IMU dataset that consists of IMU, visual signals and ARKit parameters. The resulting IMU-ARKit dataset records both signals from participants engaged in various activities, including speaking different languages, making facial expressions, speaking with emotional intonation, etc. Next, we use the IMU-ARKit dataset to train a neural network to infer facial expressions solely from IMU signals. We train a Transformer Diffusion-based neural network [41] to reliably infer Blendshape parameters directly from the IMU signals.

In addition to serving as an alternative, vision-free facial motion capture system, IMUSE enables various novel applications. In an era where digital privacy is a paramount concern, IMUSE offers a novel method to capturing facial expressions without visual input, thereby safeguarding personal visual data. In addition, by freeing a performer from holding a camera by hand towards the face, IMUSE allows facial motion capture while the performer is on the move, with normal body movements to convey body language. Finally, IMUSE can reliably conduct facial motion capture in scenarios when facial parts (e.g., the mouth) are severely occlusions (e.g., during eating or drinking), which is very challenging to vision-based solutions .

2. Related Works

Our use of IMUs for facial motion capture builds on the evolution of human motion capture technology. In the 1990s, marker-based optical motion capture technology became mainstream in the field [10, 27, 32]. Since the 2000s, advancements [18, 22, 54, 79] have enabled motion capture without special markers [42, 46, 67]. However, 3D skeletal reconstruction often requires fixed-position devices [93] or multi-camera setup [54]. This substantially constrains the range of motion and space available to the actors during capture. To address this limitation, Vlasic et al. [78] pio-

neered the use of IMUs in human motion capture, offering a more flexible and less restrictive method. Subsequently, this field witnessed rapid advancements, leading to the development of more stable systems [21, 36, 80], and the introduction of sparser configurations [82, 89].

Facial Mocap Traditional face shape representation relies on a sparse collection of 2D facial landmark points, effectively used in early works [17, 19, 20, 96]. With the growing demand for 3D visual effects, focus shifted to 3D face capture and reconstruction. In the realm of facial expression capture, Blanz and Vetter [11] proposed a novel approach using linear combinations for general face representation. In the film and visual effects industry, several studies [51, 53, 55, 64, 91] have utilized facial markers, visually tracking and computing facial expressions and motions.

These methods, however, are prohibitively expensive, location-constrained, and heavily reliant on post-production manual adjustments for consumer-level users. Marker-free approaches [7, 16, 25, 71, 83] predict facial motions from a single RGB image, reducing costs and increasing accessibility. Cao et al. [15], Paysan et al. [59] enhance the process of expression motion capture by employing various strategies to eliminate video jitter and improve robustness.

Deep learning algorithms have further advanced facial motion capture [8, 39, 58], with regression-based methods using CNNs achieving robust results from single images [30, 31, 74] or video clips [33, 40, 43, 47, 88]. Lombardi et al. [45] proposed a deep appearance model to handle complex geometry and texture in facial animation. Yoon et al. [87] improved processing images in the wild and Cao et al. [14] introduced a universal avatar prior (UAP) to train a high-resolution avatar with a mobile phone. In another way, Beeler et al. [9], Bradley et al. [12], Zhang et al. [92] developed a high-fidelity performer-specific facial capture method from multi-camera systems.

However, visually based methods [13, 83] are susceptible to occlusions. Qammaz and Argyros [62] mitigated occlusion issues by predicting information from obscured regions. Recently, facial capture based on wearable devices has shown promising results. However, all the visually based methods mentioned above face the risk of compromising user privacy due to prolonged exposure to cameras.

Sensor-based Mocap As manufacturing technology and research progresses, IMUs have seen consistent improvements. Research on the fundamental performance of IMUs calibration [6, 23, 28, 66] and correction [2, 44, 77, 78] has addressed drift issues, enhancing their stability and precision. This has made IMUs popular for body mocap applications. Video-collaborated IMU systems, developed from early works [50, 60, 61, 81], have reached high levels of accuracy [29, 35, 49, 94]. Depth cameras [34, 95], Opti-

cal markers [4] and physics constraints [3, 24, 38, 84, 85] are also common-used collaboration for IMU mocap. Efforts to reconstruct body motion using 17 IMU signals [57, 68] have led to the development of sparse IMU systems [37, 65, 70, 73]. Subsequently, the SIP [82] reduced the number of IMUs needed, while the DIP [37] achieved real-time mocap, culminating in the TransPose [86] work which refined these advancements. Compared to vision-based methods, these approaches offer significant advantages, including a wider range of motion, freedom from obstructions and lighting constraints, and benefits that are equally applicable to facial motion capture.

However, adapting this method for facial application is challenging. Commercial IMUs like noiton [57], Xsens [1], and mocopi [72] are primarily designed for body mocap and are too large and heavy for facial capture. Medina et al. [52] uses an electronic articulograph (EMA) to track tongue motion. However, the high cost makes large-scale data collection and dense sampling impractical. Advances in hardware have led to customized IMU gloves for hand posture estimation [48, 56], highlighting IMUs' potential for smaller body parts. While hand posture capture relies on detecting skeletal movements and rotational angles, facial capture involves multi-degree movements in facial regions informed by anatomical studies [75]. In our study, we leverage anatomical structures to optimize IMU placement in regions with extensive muscle motion, establishing the relationship between muscle movements and acceleration signals for effective facial capture.

3. Facial IMU

Fig. 1 provides an overview of IMUSE. The left section outlines our data collection process. Participants are requested to wear multiple IMUs and perform a range of facial expressions and motions to capture corresponding signals. We designed these compact flexible electronic material IMUs to attach to the face simultaneously without impeding facial movements. In the middle section, we illustrate our network's data processing workflow. The collected IMU data is first aligned to a unified coordinate system using calibration. Then we establish an IMU2Face model that reconstructs facial actions based on the aligned IMU signals. The right section highlights the potential applications of IMUSE, offering solutions to address some limitations of visual-based facial capture.

Within the field of motion capture, IMU plays a critical role in reflecting the spatial movements of an object by measuring its orientation and acceleration. IMUs designed for full-body motion capture, such as Xsens, Sony Mocopi and others, have been widely applied commercially. These units usually consist of various parts, including detecting sensors and data transmission modules, making them too hulking to be used for facial motion capture. Furthermore, employ-

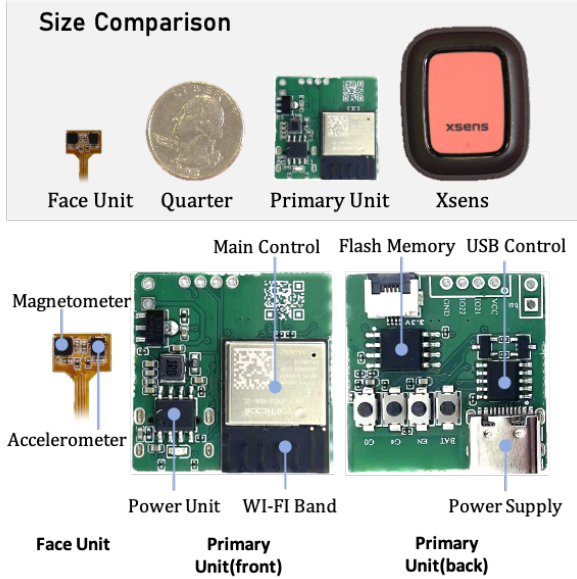


Figure 2. Our IMU has two main components: the face unit and the primary unit. Top: size comparison. Bottom: architecture design.

ing multiple units of this model for facial capture can lead to severe occlusion, preventing observation of the participant’s facial expressions. This necessitates the development of a custom-designed IMU, specifically tailored to meet the unique requirements and scale of facial motion capture.

Our design preserves the function of standard IMU while minimizing weight and size to cater to the requirements for facial capture. Fig. 2 (top) compares the size of our IMU. We achieved significant miniaturization by separating the sensor module from the data transmission module. We designed the IMU’s face module using flexible electronic materials to closely conform to the skin, ensuring that it does not impede the wearer’s facial movements. This design allowed our sensor module to be exceptionally compact, measuring only 0.6 cm² and weighing merely 0.3 grams, a stark reduction to 5.4% of the Xsens module’s area and only 2.7% of its weight.

3.1. Facial IMU Sensor

Fig. 2(down) provides a detailed overview of the specific hardware components utilized in our study. The sensor module incorporates a total of nine-axis sensing sub-units, which include the QMC5883P [63] from Silicon Power, a three-axis magnetic field sensor with a measurement range of ± 30 gauss, and the QMI8658 [63] integrated chip, which combines a three-axis gyroscope and accelerometer. These sensors are capable of accurately recording spatial positions and accelerations at a rate of 60fps. The data transmission module is primarily based on the ESP32 controller. It em-

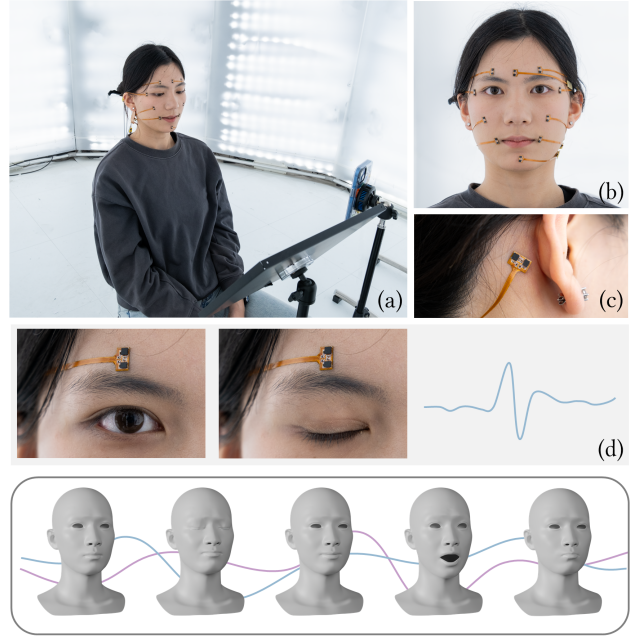


Figure 3. IMU-ARKit dataset collection settings. Upper: (a) Our capture setup, including the iPhone for ARKit signal capture, teleprompter, and facial IMUs. (b) IMU layout. (c) IMU placed behind the ear to record head rotation. (d) Sample signal corresponding to a blink. Lower: Pairwisely ARKit and IMU dataset.

plies the UDP protocol to collect and correct data detected by the sensor module. Additionally, we use a Wi-Fi module to transmit the computed data to the host computer. This data includes time stamps, quaternion representations, and acceleration values at each recorded instance.

The data transmission module of our Face IMU sensor system requires only a 5V battery supply. This setup provides the essential conditions for the portability and wearability of the Face IMU sensor system. Furthermore, as the connection to the host computer is via Wi-Fi, users can move freely within the Wi-Fi signal range while wearing the Face IMU, enabling high degrees of mobility.

Fig. 3 exemplifies the remarkable sensitivity of our IMU in capturing even the most minute motion signals. In this demonstration, a participant wearing an IMU detector on the eyebrow performs subtle blink movements. In the waveform diagram shown in (d), we can clearly see a complete motion sequence: starting with the initial acceleration as the eyebrow begins its ascent, followed by a deceleration phase as the movement slows, and culminating in a stationary phase when the eyebrow ceases to move. The graph distinctly demarcates these stages, underscoring the precision with which our IMU detects even the most delicate movements. Our supplementary video provides a more dynamic visualization of the motion.

3.2. Synchronization and Calibration

We delved deeply into the essential technology for capturing facial information in synchrony using multiple IMUs. To achieve this, it is imperative to address two fundamental challenges: synchronization and calibration. We designated one ESP32 as the auxiliary ESP32, employing it as a benchmark for synchronizing and calibrating the others. To ensure coherent and coordinated data collection from these diverse sensors, we integrated a calibration program into this ESP32 within the data transfer module during hardware design. Before data acquisition by the IMUs, we used the data module of the auxiliary ESP32’s clock as a reference point. We transmitted pulse signals through the DuPont line to each IMU’s ESP32 for calibration purposes. Upon receiving this pulse signal, each ESP32 aligns its internal clock with the external reference, synchronizing the timestamps across all IMUs. With these synchronized signals, we obtain the raw signals $\dagger\mathcal{S} = \{\dagger\mathcal{R}, \dagger\mathcal{A}\}$ from all the n IMUs, where $\dagger\mathcal{R} = \{\dagger\mathcal{R}^0, \dagger\mathcal{R}^1, \dots, \dagger\mathcal{R}^n\}$ represent the rotation matrix sequence of the number i IMU, and $\dagger\mathcal{A} = \{\dagger\mathcal{A}^0, \dagger\mathcal{A}^1, \dots, \dagger\mathcal{A}^n\}$ represent the acceleration sequence of the number i IMU. The rotation matrix represents the rotation from the IMU’s local coordinate system to the world coordinate system. Notably, we denote the index of the auxiliary IMU as 0. For ease of subsequent analyses, we initially convert the acceleration from the local coordinate system to the world coordinate system. For the IMU i ’s data on the frame j , we denote the raw acceleration and orientations as $\dagger a_j^i$ and $\dagger R_j^i$. The world coordinate acceleration can be represented as:

$$a_j^i = (\dagger R_j^i)^{-1} \dagger a_j^i. \quad (1)$$

Next, acknowledging the variability in facial structures and the potential for slight discrepancies in IMU placement each time, we adopted the concept of a Neutral facial performance, similar to the approach used by [25, 86] in body mocap. After wearing the IMUs for the participants, we had each participant relax the facial muscles, presenting a Neutral state, and recorded the orientation of each IMU $\{R_{\text{neutral}}^i\}$. In subsequent calculations, we used the orientation relative to this pose as a baseline:

$${}^*R_j^i = (R_{\text{neutral}}^i)^{-1} \dagger R_j^i. \quad (2)$$

Considering that two types of movements influence an IMU’s signal when placed on the face — the overall movement of the head and the movements caused by facial expressions. Our focus is on deducing expressions from IMU signals. As illustrated in Fig. 3 (b), not only do we deploy IMUs across the facial region, but we also strategically place an auxiliary IMU behind the ear, as shown in (c). This placement is specifically designed to mitigate the impact of

general head movements on the orientations and accelerations detected by the other IMUs. For convenience, we define the index of the auxiliary IMU to be 0. The calibrated IMU rotation can be expressed as

$$R_j^i = \begin{cases} ({}^*R_0^i)^{-1} {}^*R_j^i & \text{if } j \neq 0, \\ {}^*R_0^i & \text{otherwise} \end{cases} \quad (3)$$

We denote the calibrated IMU signal as $\mathcal{S} = \{\mathcal{R}, \mathcal{A}\}$.

4. IMU-based Facial Motion Capture

4.1. IMU Placement and Anatomic Guidance

To accurately capture facial movements, it is imperative to attach IMUs to distinct regions on the surface of the face. In the left panel of Fig. 3, we present our strategic arrangement of IMUs. This layout is informed by a detailed analysis of the distribution of facial muscles[75]. We demarcated distinct facial zones, referencing key anatomical landmarks including: the zygomaticus area, crucial for expressing emotions like joy or sorrow; the buccinator and mentalis area, fundamental for movements pertinent to speech; the orbicularis oculi area, important for a spectrum of expressions such as smiling and frowning; and the frontalis area, integral for conveying sentiments such as dissatisfaction or melancholy. In every designated region, we meticulously placed at least one IMU to ensure comprehensive monitoring of the key muscle groups and facial zones. Additionally, in regions characterized by dense muscle presence or complex movements, we opted for dual IMU placement. This approach is exceptionally effective in capturing a complete range of muscle movements in these specific areas.

Furthermore, our design strategy was acutely focused on minimizing the IMUs’ impact on both the natural facial movements and the comfort of our participants. Acknowledging the sensitivity of certain facial regions, we intentionally avoided placing IMUs on the eyelids and the corners of the mouth, as these areas are not only crucial for a wide range of expressions but are also prone to discomfort if constrained. The wiring was also thoughtfully routed along the periphery of the face to avoid interfering with the participant’s expressions and to preserve the clarity of any accompanying visual data. These measures enabled us to maintain the fidelity of the IMU data and any visual records while respecting the comfort and expressiveness of the participants.

4.2. Capturing IMU-ARKit Dataset

Blendshape technology is widely used in the realm of facial animation and motion capture due to its ability to generate highly realistic and nuanced expressions. This technology operates on the principle of parametric modeling. Specifically, a blendshape model is defined by a collection of blendshape weights, denoted as $\mathcal{W} =$

$\{w_1, w_2, \dots, w_m\}$, a blendshape model can be represented as:

$$M(\mathcal{W}) = B_0 + \sum_k^m w_k B_k. \quad (4)$$

where B_0 represents the neutral face, B_k is the blendshape basis vector, and m is the number of blendshapes. By linearly interpolating between different blend shapes, this approach allows for the creation of multiple facial expressions.

Our challenge is to derive these blend shape parameters \mathcal{W} from the IMU data \mathcal{S} . Given that the IMU is capable of capturing motion and orientation, we propose a method for mapping these physical measurements to blend shape coefficients. This requires the development of an algorithm that converts IMU readings into meaningful hybrid shape parameters.

In order to realize a data-driven solution for predicting facial blendshape weights using IMU, we set out to create a facial IMU with the ARKit dataset, as demonstrated in the bottom of Fig. 3 This dataset was carefully compiled to contain paired data from IMU and ARKit to ensure a comprehensive base for model training.

Our dataset contains records from 20 different participants. These individuals are all in the 18-40 age range, proficient in English, and have some background in acting, thus providing richly varied and vivid facial expressions. The left panel of Fig. 3(a) shows an example of the data collection setup. We installed a set of 11 IMU detectors for each participant and sat in the acquisition seat, with the teleprompter screen placed directly in front of the participant, next to an iPad that captured the visual information. the iPad used LiveLinkface [76] to capture the visual information, and the captured visual signals were divided into two parts: the RGB video sequence and the ARKit Parameters.

Before the formal data collection process began, participants were given time to acclimatize to the sensation of wearing the IMU to ensure natural and unrestricted facial movements. Participants then gently triple-clicked the IMU located on mentalis, which was used at a later stage to synchronize the IMU signals with the visual signals. Data collection for each participant was divided into three different sections, each preceded by a sample video for the participant to mimic. In the first section, participants read aloud the provided content in a calm tone, with a split between native language and English. This was done to capture the natural facial movements associated with the language. In the second session, participants were asked to read aloud the same content, but with a specific emotion consistent with the context of the script, thus adding emotional layers to the facial expressions. Finally, the third segment asked participants to sequentially make a series of facial expressions that

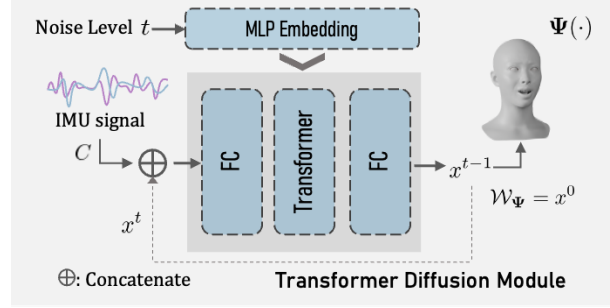


Figure 4. Our transformer diffusion network architecture. We use IMU signal C as a condition input to the network. In each iteration, the network denoises x , and the final network output, x_0 , is the predicted blendshape parameters.

were based on specific classifications, ensuring a full range of emotions and movements.

4.3. IMU Based Facial Tracker

In this study, a novel data flow was established, as depicted in Fig. 4. Initially, a calibration process was applied to the raw IMU-ARKit data. This procedure was instrumental in generating paired data sets of IMU-ARKit parameters, which were subsequently utilized for the training of the network.

The network ingests calibrated IMU data as its input. To simplify the inputs to the network, we first express the rotations R_j^i as quaternions $q_j^i \in \mathbb{R}^4$. We concatenate q_j^i with a_j^i , denoted as $c_j^i \in \mathbb{R}^7$, and then concatenate all 11 IMUs' signal as $C_j = [c_1, c_2, \dots, c_n] \in \mathbb{R}^{77}$. These inputs are meticulously calibrated, ensuring both the accuracy and reliability of the IMU signals. In detail, for each frame j of imu i , we convert the rotation matrix R_j^i into quaternion, and then put it together with the acceleration to form a 7-dimensional vector. We combine the signals from 11 IMUs in 120 consecutive frames to $C_j \in \mathbb{R}^{77 \times 120}$ that serves as the input to the network.

Our network $\Psi(\cdot)$ comprises three critical components: an initial Fully Connected (FC) layer, a transformer-based diffusion core, a concluding FC layer, and an MLP embedding network. We denote the two FC layer and the transformer-based diffusion core as $\psi(\cdot)$.

Our network is intricately designed around a diffusion architecture. Central to its operation is the concept of iterative denoising, a process repeated n times to achieve the final predicted 120 frames' blendshape weights $\mathcal{W}_{\Psi,j} \in \mathbb{R}^{55 \times 120}$.

At the outset of this process, we set x_j^n as a random noise that has the same dimension with $\mathcal{W}_{\Psi,j}$. For the t iteration, we feed the integer t into the MLP Embedding module. Then, the IMU signal C_j for the condition is concatenated with x_j^t and fed into the ψ network along with the embedding output, to calculate x_j^{t-1} :

$$x_j^{t-1} = \psi(\text{MLP}(t), x_j^t, \mathbf{C}_j). \quad (5)$$

We iteratively compute until we get x_j^0 as the predicted blendshape weights $\mathcal{W}_{\Psi,j}$.

Throughout the training process, ground truth ARKit parameters \mathcal{W}_j serve for supervision. We assess the network’s performance using an L1 loss function,

$$\mathcal{L} = |\mathcal{W}_{\Psi} - \mathcal{W}|. \quad (6)$$

The equation evaluates the accuracy of the network’s outputs against these ground truth parameters.

We trained our network in a supervised manner on the IMU-ARKit dataset. During the training phase, we used any continuous 120 frames from the training set as the network’s input to predict the corresponding 120 ARKit parameters. In the testing phase, after each prediction, we used the last 60 frames in the current time window along with the next 60 frames as the next input for the network. This approach ensures that the network has sufficient prior information to accurately determine the initial state of the face within this time window.

5. Experimental Evaluations

In Fig. 6, we use IMUSE to recover a variety of facial expressions. We include sequences of facial expressions that represent signature emotions as well as sequences of a performer speaking. The video results can be found in the supplementary video.

Following the similar network architecture as Li et al. [41], IMUSE uses the noise as inputs, imposes the IMU data as transformer conditions, and outputs the inferred blendshape weights to control facial motions. We use Adam as the optimizer with a learning rate 2×10^{-4} , $\alpha = 0.9$, $\beta = 0.999$. We train and evaluate IMUSE on a single NVIDIA RTX3090 GPU. The training process takes ≈ 1 hours on all identities with paired data. For the generation and rendering of facial assets, we leverage the off-the-shelf technique DreamFace [90] to maintain high fidelity and realistic results.

5.1. Evaluations on IMU Locations

We qualitatively evaluate how IMU placements across different facial regions affect final facial expression estimation, as shown in Fig. 7. The far left image compares various IMU position schemes, with white dots on the face representing the final locations IMUSE uses. The images, arranged from left to right, depict the experimental positioning of test points in the Frontalis Area, Zygomaticus Area, and Buccinator and Mentalis Area, respectively. The top row shows the locations we have experimented with for placing the IMUs, with the red and purple ones as the final positions we chose to use.

Table 1. Quantitative ablation study of our method.

Method	PVE [mm]↓	PVE_LMK [mm]↓	MSE↓
Ours	0.075 ± 0.055	0.126 ± 0.091	0.0075
<i>Small Dataset</i>	0.089 ± 0.063	0.150 ± 0.102	0.0093
<i>Fewer IMU</i>	0.078 ± 0.055	0.129 ± 0.089	0.0082

Table 2. Quantitative evaluations on IMU placements. The table shows the variations times 10^{-3} where higher value essentially corresponds to higher sensitivity. Numbers in **Bold** fonts correspond to the placements that IMUSE uses.

Area	#1	#2	#3	#4	#5
Frontalis	0.71	0.57	0.52	0.58	-
Zygomaticus	0.64	1.20	0.57	0.32	-
Buccinator / Mentalis	0.84	1.38	0.54	0.88	1.77

In our studies, we strategically select the candidates for placing the IMUS to best reduce interference as well as to align with the underlying muscles. The middle row demonstrates the specific facial movements performed by participants wearing the IMUs. We collect the acceleration data from respective IMUs during specific facial movements, shown in the bottom row of the images. Our selected IMU locations unanimously produce strong signals that correspond to higher sensitivity under motion. Such placements result in signals with a high SNR suitable for recovering accurate and reliable facial motions. Table 2 further shows the quantitative results.

5.2. Evaluations on Facial Capture

Next, we compare IMUSE with the state-of-the-art vision-based techniques DECA [26] and 3DDFA_V2 [30]. Specifically, we experiment on a new IMU-ARKit dataset that takes the iPhone captured image as the input of DECA and 3DDFA_V2 along with IMUSE. The results are shown in Fig. 8. Columns 3, 6, and 7 correspond to the results from IMUSE vs. 3DDFA_V2 and DECA. Visual quality wise, IMUSE estimations are comparable to the SOTA visual-based methods. Compared with DECA, IMUSE performs better near the eye region. Compared with 3DDFA_V2, IMUSE better recovers eyebrow movements induced by facial expressions.

We further conduct two ablation experiments to evaluate our dataset and the IMU placements: (1) *Fewer IMU*: we train the network using only a fraction of IMUs, i.e., the ones placed on the eyebrows (2 IMUs), jaw (1 IMU), and cheeks (2 IMUs). (2) *Small Dataset*: we train the network using 1/3 of the dataset.

The variations are illustrated in columns 4, and 5 of Fig. 8 sequentially. The results in column 4 show some examples that IMUSE fails to faithfully predict the motion, e.g., closed eyes. This is largely attributed to the locations

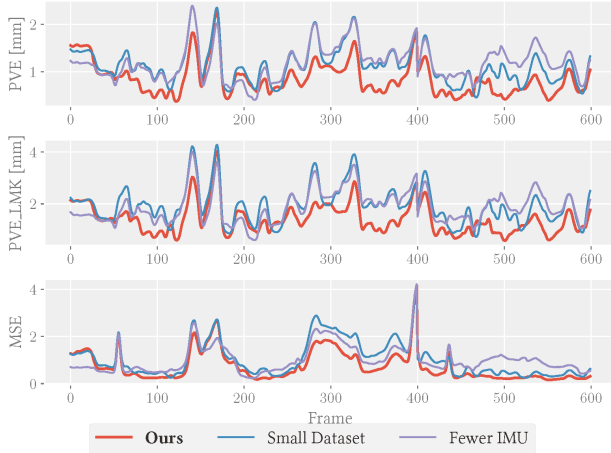


Figure 5. Quantitative result of our method on test data. We plot the PVE, PVE.LMK and MSE calculated per frame with ARKit as ground truth on a sequence.

where we place the IMUs. The results in column 5 manage to recover challenging facial distortions under extreme expressions. This indicates that our training dataset is sufficiently rich to cover these movements and the trained network is robust enough to generalize to reproduce these distortions.

We further conduct quantitative evaluations in Fig. 5 and Table. 1. Same as [26, 30], we calculate the 3D per vertex error (PVE)[69] on the deformed mesh as an indicator of the similarity between ARKit vs. IMUSE predictions. Specifically, we use the 3D landmark vertex error (PVE.LMK) to demonstrate the fidelity of IMUSE estimations on visually significant areas. We further calculate the MSE using the predicted blendshape weights with ARKit as the ground truth. The red curve represents the metrics for each frame using IMUSE whereas the purple and blue curves represent the metrics for the two ablation experiments.

5.3. Potential Applications.

Camera-Free Facial Capture. In traditional facial capture systems, users need to always face the camera, which limits the head and body movements. For example, while on the move, users have to hold their phones by hand, making it difficult to perform normal body movements and convey body language. We demonstrate using IMUSE a portable facial capture solution, as shown in the left of Fig. 9. Due to the modular design of the IMUs, the user’s facial skin experiences minimal weight. We use a portable power bank to supply power to all IMUs and a Wi-Fi module to communicate with the computer. As a result, IMUSE allows for accurate facial capture while a person is walking, preserving complete facial information and freeing the user’s hands. The supplementary video includes several dynamic

sequences.

Occluded Facial Capture. In some scenarios, facial capture encounters unavoidable occlusions, such as during eating or drinking. Professional actors commonly resort to ‘mimicking’ eating to avoid this issue, which can result in a lack of authenticity. We demonstrate using IMUSE to conduct robust motion capture in such scenarios. We showcase IMUSE’s accurate and stable motion capture capabilities in the heavily occluded ‘eating an apple’ situation, as shown in the right of Fig. 9. When eating, the user’s hands and the food largely occlude the face, particularly the mouth regions, rendering vision-based methods ineffective. IMUSE, instead, does not rely on any video signals, allowing for accurate capture of the mouth movements.

6. Discussions and Future Work

We have presented IMUSE, a novel vision-free facial motion capture technique, that directly recovers facial motions from merely IMU signals. In IMUSE, our tailored micro-IMUs are strategically attached to facial regions aligned with facial anatomy, to capture a wide spectrum of facial movements, from nuanced to dramatic. We have developed a companion learning-based framework for reliable motion inference as well as acquired a hybrid IMU-ARKit dataset with synchronized IMU and visual signals of diverse facial expressions from various performers. The IMUSE design, datasets and code will be released to the community for comprehensive evaluations.

In today’s digital landscape, privacy concerns are increasingly at the forefront. The surge in popularity of virtual platforms underscores the necessity of safeguarding user anonymity and privacy. However, traditional facial animation methods predominantly hinge on visual data capture, typically necessitating model localization via camera-based systems. These methods, reliant on visual inputs to track facial movements, can inadvertently breach privacy. IMUSE in contrast obviates the need for direct visual capture of the face, potentially upholding user privacy by avoiding the capture and storage of visual facial data. Furthermore, with IMUSE, factors like lighting conditions or the orientation of the face may no longer be impediments.

IMUSE has also benefited from the technological advances of material science and integrated circuits where IMU-like prototypes are becoming cheaper, smaller, safer, and more pervasive. More importantly, IMUSE showcases the potential of using flexible electronic materials [56] for providing more user-friendly and wearable solutions with electronic materials. In fact, in our earlier attempt without flexible electronics, we had to attach the signal detection module the facial skins of the performer with double-sided and adhesive tapes, causing strong discomforts to the performer. IMUSE alleviates this discomfort but still leaves

space for future, more clever designs. Indeed, it is our hope that IMUSE will stimulate significant future developments on IMU-based facial motion capture, echoing recent successes in IMU body motion capture.

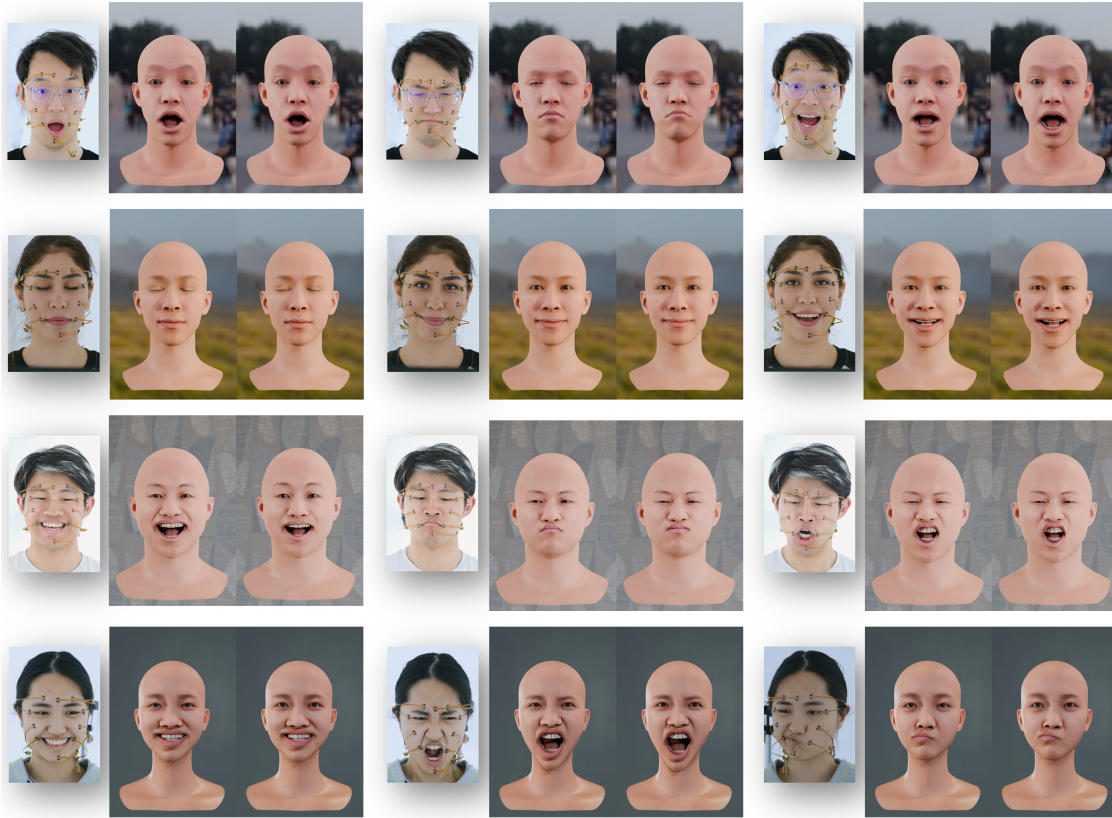


Figure 6. Gallery. We present four subjects, with each row corresponding to three different expressions of a single participant. For each subfigure, Left: Image reference. Middle: Facial motion reconstructed by our pipeline. Right: Recorded result by ARKit[5]. Our method achieves results that are comparable to those obtained using ARKit.

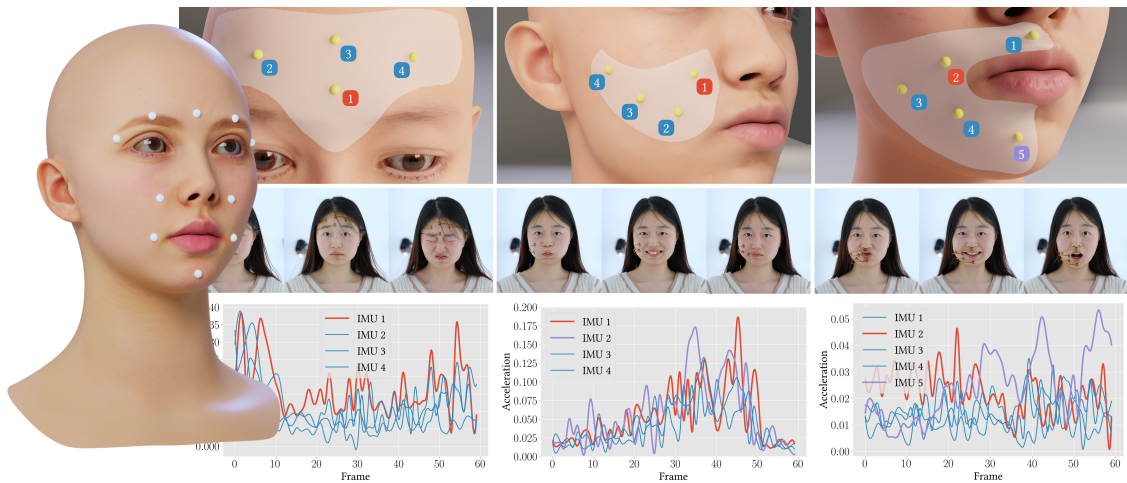


Figure 7. Experiment on IMU placement on the face. This figure presents our anatomically-based facial partitioning, highlighting the selected points and the corresponding experiments conducted for each facial region. The left image shows our chosen points on the face, while the other images elaborate on the individual experiments conducted for each specific area. The upper section presents a distribution map of the test points allocated to each region, the middle section identifies the primary expressions and movements associated with that area, and the lower section exhibits the acceleration curves of the IMUs situated at each designated point.

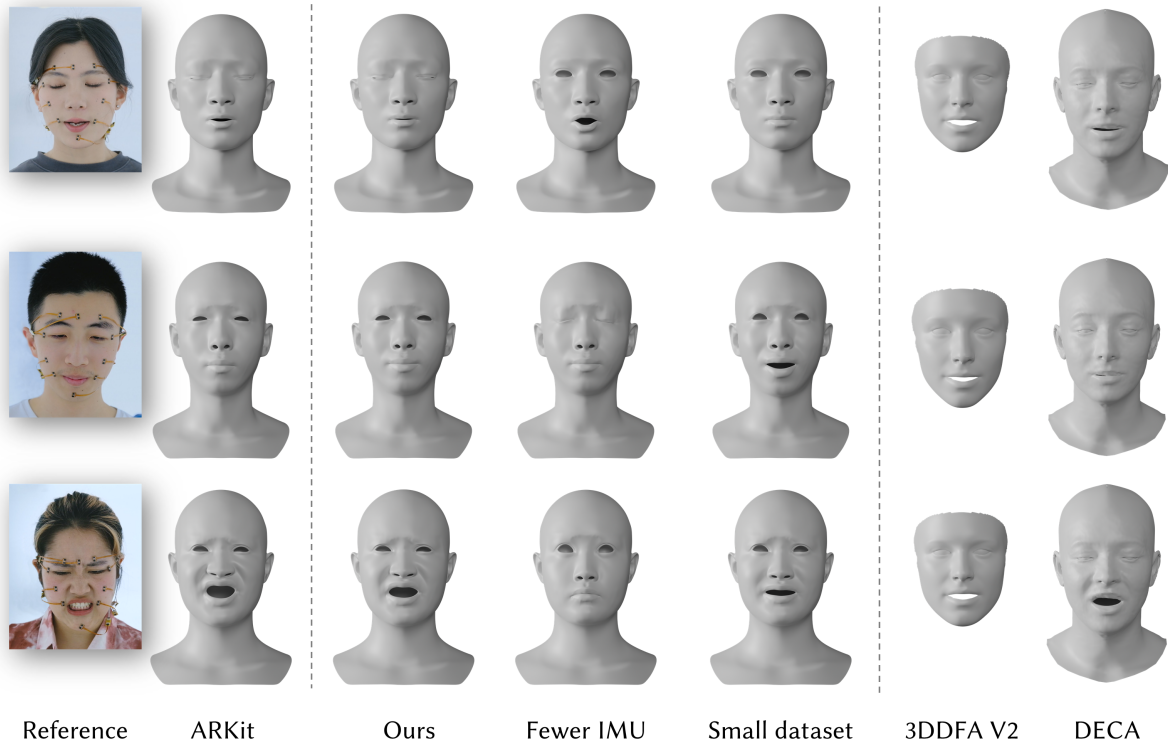


Figure 8. Qualitative comparison and ablation study. The first column displays the reference image. The second column illustrates the record result by ARKit [5]. The third column shows the reconstruction results of our pipeline. Columns 5 and 6 illustrate the result of our ablation experiment *Fewer IMU* and *Small Dataset* respectively. Columns 6 and 7 illustrate the results of 3DDFA V2 [30] and DECA [26] respectively.

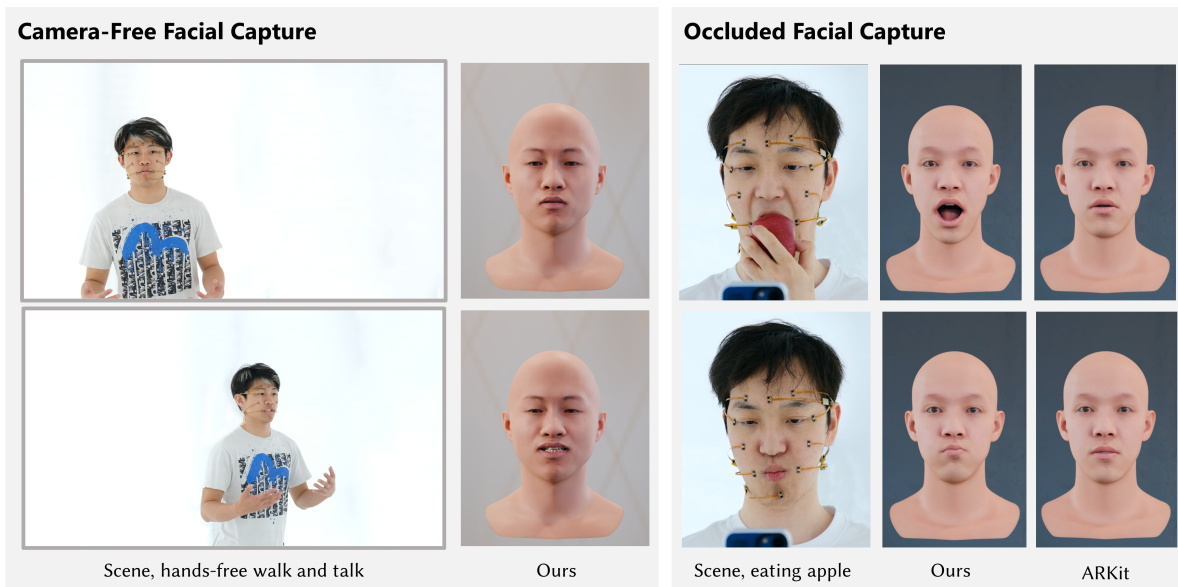


Figure 9. Applications. Left: Camera-Free facial capture. Right: Facial capture during occlusions.

References

- [1] 2023. Xsens products. <https://www.movella.com/products/xsens#products/>.
- [2] Norhafizan Ahmad, Raja Ariffin Raja Ghazilla, Nazirah M Khairi, and Vijayabaskar Kasi. 2013. Reviews on various inertial measurement unit (IMU) sensor applications. *International Journal of Signal Processing Systems* 1, 2 (2013), 256–262.
- [3] Sadeqh Aliakbarian, Pashmina Cameron, Federica Bogo, Andrew Fitzgibbon, and Thomas J Cashman. 2022. Flag: Flow-based 3d avatar generation from sparse observations. In *Proceedings of the IEEE/CVF Conference on Computer Vision and Pattern Recognition*. 13253–13262.
- [4] Sheldon Andrews, Ivan Huerta, Taku Komura, Leonid Sigal, and Kenny Mitchell. 2016. Real-time physics-based motion capture with sparse sensors. In *Proceedings of the 13th European conference on visual media production (CVMP 2016)*. 1–10.
- [5] Apple. 2023. ARKit. <https://developer.apple.com/arkit/>.
- [6] Eric R Bachmann, Robert B McGhee, Xiaoping Yun, and Michael J Zyda. 2001. Inertial and magnetic posture tracking for inserting humans into networked virtual environments. In *Proceedings of the ACM symposium on Virtual reality software and technology*. 9–16.
- [7] Linchao Bao, Xiangkai Lin, Yajing Chen, Haoxian Zhang, Sheng Wang, Xuefei Zhe, Di Kang, Haozhi Huang, Xinwei Jiang, Jue Wang, et al. 2021. High-fidelity 3D digital human head creation from RGB-D selfies. *ACM Transactions on Graphics (TOG)* 41, 1 (2021), 1–21.
- [8] Júlio César Batista, Vítor Albiero, Olga RP Bellon, and Luciano Silva. 2017. Aumpnet: simultaneous action units detection and intensity estimation on multi-pose facial images using a single convolutional neural network. In *2017 12th IEEE international conference on automatic face & gesture recognition (FG 2017)*. IEEE, 866–871.
- [9] Thabo Beeler, Fabian Hahn, Derek Bradley, Bernd Bickel, Paul A Beardsley, Craig Gotsman, Robert W Sumner, and Markus H Gross. 2011. High-quality passive facial performance capture using anchor frames. *ACM Trans. Graph.* 30, 4 (2011), 75.
- [10] L Bianchi, D Angelini, GP Orani, and F Lacquaniti. 1998. Kinematic coordination in human gait: relation to mechanical energy cost. *Journal of neurophysiology* 79, 4 (1998), 2155–2170.
- [11] V Blanz and T Vetter. 1999. A Morphable Model for the Synthesis of 3D Faces. In *26th Annual Conference on Computer Graphics and Interactive Techniques (SIGGRAPH 1999)*. ACM Press, 187–194.
- [12] Derek Bradley, Wolfgang Heidrich, Tiberiu Popa, and Alla Sheffer. 2010. High resolution passive facial performance capture. In *ACM SIGGRAPH 2010 papers*. 1–10.
- [13] Chen Cao, Derek Bradley, Kun Zhou, and Thabo Beeler. 2015. Real-time high-fidelity facial performance capture. *ACM Transactions on Graphics (TOG)* 34, 4 (2015), 1–9.
- [14] Chen Cao, Tomas Simon, Jin Kyu Kim, Gabe Schwartz, Michael Zollhoefer, Shun-Suke Saito, Stephen Lombardi, Shih-En Wei, Danielle Belko, Shoou-I Yu, et al. 2022. Authentic volumetric avatars from a phone scan. *ACM Transactions on Graphics (TOG)* 41, 4 (2022), 1–19.
- [15] Chen Cao, Yanlin Weng, Stephen Lin, and Kun Zhou. 2013. 3D shape regression for real-time facial animation. *ACM Transactions on Graphics (TOG)* 32, 4 (2013), 1–10.
- [16] Chen Cao, Yanlin Weng, Shun Zhou, Yiyong Tong, and Kun Zhou. 2013. Facewarehouse: A 3d facial expression database for visual computing. *IEEE Transactions on Visualization and Computer Graphics* 20, 3 (2013), 413–425.
- [17] Xudong Cao, Yichen Wei, Fang Wen, and Jian Sun. 2014. Face alignment by explicit shape regression. *International journal of computer vision* 107 (2014), 177–190.
- [18] Zhe Cao, Tomas Simon, Shih-En Wei, and Yaser Sheikh. 2017. Realtime multi-person 2d pose estimation using part affinity fields. In *Proceedings of the IEEE conference on computer vision and pattern recognition*. 7291–7299.
- [19] Timothy F. Cootes, Gareth J. Edwards, and Christopher J Taylor. 2001. Active appearance models. *IEEE Transactions on pattern analysis and machine intelligence* 23, 6 (2001), 681–685.
- [20] Timothy F Cootes, Christopher J Taylor, David H Cooper, and Jim Graham. 1995. Active shape models—their training and application. *Computer vision and image understanding* 61, 1 (1995), 38–59.
- [21] Juan Antonio Corrales, Francisco A Candelas, and Fernando Torres. 2008. Hybrid tracking of human operators using IMU/UWB data fusion by a Kalman filter. In *Proceedings of the 3rd ACM/IEEE international conference on Human robot interaction*. 193–200.
- [22] Edilson de Aguiar, Christian Theobalt, Marcus Magnor, Holger Theisel, and H-P Seidel. 2004. M/sup 3: marker-free model reconstruction and motion tracking from 3D voxel data. In *12th Pacific Conference on Computer Graphics and Applications, 2004. PG 2004. Proceedings*. IEEE, 101–110.
- [23] Michael B Del Rosario, Heba Khamis, Phillip Ngo, Nigel H Lovell, and Stephen J Redmond. 2018. Com-

- putationally efficient adaptive error-state Kalman filter for attitude estimation. *IEEE Sensors Journal* 18, 22 (2018), 9332–9342.
- [24] Andrea Dittadi, Sebastian Dziadzio, Darren Cosker, Ben Lundell, Thomas J Cashman, and Jamie Shotton. 2021. Full-body motion from a single head-mounted device: Generating smpl poses from partial observations. In *Proceedings of the IEEE/CVF International Conference on Computer Vision*. 11687–11697.
- [25] Bernhard Egger, William AP Smith, Ayush Tewari, Stefanie Wuhrer, Michael Zollhoefer, Thabo Beeler, Florian Bernard, Timo Bolkart, Adam Kortylewski, Sami Romdhani, et al. 2020. 3d morphable face models—past, present, and future. *ACM Transactions on Graphics (ToG)* 39, 5 (2020), 1–38.
- [26] Yao Feng, Haiwen Feng, Michael J Black, and Timo Bolkart. 2021. Learning an animatable detailed 3D face model from in-the-wild images. *ACM Transactions on Graphics (ToG)* 40, 4 (2021), 1–13.
- [27] Giancarlo Ferrigno, NA Borghese, and Antonio Pedotti. 1990. Pattern recognition in 3D automatic human motion analysis. *ISPRS Journal of Photogrammetry and Remote Sensing* 45, 4 (1990), 227–246.
- [28] Eric Foxlin. 1996. Inertial head-tracker sensor fusion by a complementary separate-bias Kalman filter. In *Proceedings of the IEEE 1996 Virtual Reality Annual International Symposium*. IEEE, 185–194.
- [29] Andrew Gilbert, Matthew Trumble, Charles Malleson, Adrian Hilton, and John Collomosse. 2019. Fusing visual and inertial sensors with semantics for 3d human pose estimation. *International Journal of Computer Vision* 127 (2019), 381–397.
- [30] Jianzhu Guo, Xiangyu Zhu, Yang Yang, Fan Yang, Zhen Lei, and Stan Z Li. 2020. Towards fast, accurate and stable 3d dense face alignment. In *European Conference on Computer Vision*. Springer, 152–168.
- [31] Yudong Guo, Jianfei Cai, Boyi Jiang, Jianmin Zheng, et al. 2018. Cnn-based real-time dense face reconstruction with inverse-rendered photo-realistic face images. *IEEE transactions on pattern analysis and machine intelligence* 41, 6 (2018), 1294–1307.
- [32] Yan Guo, Gang Xu, and Saburo Tsuji. 1994. Understanding human motion patterns. In *Proceedings of the 12th IAPR International Conference on Pattern Recognition, Vol. 3-Conference C: Signal Processing (Cat. No. 94CH3440-5)*, Vol. 2. IEEE, 325–329.
- [33] Marc Habermann, Weipeng Xu, Michael Zollhoefer, Gerard Pons-Moll, and Christian Theobalt. 2019. Livecap: Real-time human performance capture from monocular video. *ACM Transactions On Graphics (TOG)* 38, 2 (2019), 1–17.
- [34] Thomas Helten, Meinard Muller, Hans-Peter Seidel, and Christian Theobalt. 2013. Real-time body tracking with one depth camera and inertial sensors. In *Proceedings of the IEEE international conference on computer vision*. 1105–1112.
- [35] Roberto Henschel, Timo Von Marcard, and Bodo Rosenhahn. 2020. Accurate long-term multiple people tracking using video and body-worn IMUs. *IEEE Transactions on Image Processing* 29 (2020), 8476–8489.
- [36] Fuyang Huang, Ailing Zeng, Minhao Liu, Qiuxia Lai, and Qiang Xu. 2020. DeepFuse: An IMU-aware network for real-time 3D human pose estimation from multi-view image. In *Proceedings of the IEEE/CVF Winter Conference on Applications of Computer Vision*. 429–438.
- [37] Yinghao Huang, Manuel Kaufmann, Emre Aksan, Michael J Black, Otmar Hilliges, and Gerard Pons-Moll. 2018. Deep inertial poser: Learning to reconstruct human pose from sparse inertial measurements in real time. *ACM Transactions on Graphics (TOG)* 37, 6 (2018), 1–15.
- [38] Jiayi Jiang, Paul Streli, Huajian Qiu, Andreas Fender, Larissa Laich, Patrick Snape, and Christian Holz. 2022. Avatarposer: Articulated full-body pose tracking from sparse motion sensing. In *European Conference on Computer Vision*. Springer, 443–460.
- [39] Samuli Laine, Tero Karras, Timo Aila, Antti Herva, Shunsuke Saito, Ronald Yu, Hao Li, and Jaakko Lehtinen. 2017. Production-level facial performance capture using deep convolutional neural networks. In *Proceedings of the ACM SIGGRAPH/Eurographics symposium on computer animation*. 1–10.
- [40] Hao Li, Laura Trutoiu, Kyle Olszewski, Lingyu Wei, Tristan Trutna, Pei-Lun Hsieh, Aaron Nicholls, and Chongyang Ma. 2015. Facial performance sensing head-mounted display. *ACM Transactions on Graphics (ToG)* 34, 4 (2015), 1–9.
- [41] Jiaman Li, Karen Liu, and Jiajun Wu. 2023. Ego-Body Pose Estimation via Ego-Head Pose Estimation. In *Proceedings of the IEEE/CVF Conference on Computer Vision and Pattern Recognition*. 17142–17151.
- [42] Yuwei Li, Minye Wu, Yuyao Zhang, Lan Xu, and Jingyi Yu. 2021. PIANO: A Parametric Hand Bone Model from Magnetic Resonance Imaging. *arXiv preprint arXiv:2106.10893* (2021).
- [43] Daizong Liu, Hongting Zhang, and Pan Zhou. 2021. Video-based facial expression recognition using graph convolutional networks. In *2020 25th International Conference on Pattern Recognition (ICPR)*. IEEE, 607–614.
- [44] Huajun Liu, Xiaolin Wei, Jinxiang Chai, Inwoo Ha, and Taehyun Rhee. 2011. Realtime human motion control with a small number of inertial sensors. In

Symposium on interactive 3D graphics and games. 133–140.

- [45] Stephen Lombardi, Jason Saragih, Tomas Simon, and Yaser Sheikh. 2018. Deep appearance models for face rendering. *ACM Transactions on Graphics (ToG)* 37, 4 (2018), 1–13.
- [46] Matthew Loper, Naureen Mahmood, Javier Romero, Gerard Pons-Moll, and Michael J Black. 2015. SMPL: A Skinned Multi-Person Linear Model. *ACM Transactions on Graphics* 34, 6 (2015).
- [47] Luming Ma and Zhigang Deng. 2019. Real-time hierarchical facial performance capture. In *Proceedings of the ACM SIGGRAPH Symposium on Interactive 3D Graphics and Games*. 1–10.
- [48] Oleg Makaussov, Mikhail Krassavin, Maxim Zhabinets, and Siamac Fazli. 2020. A low-cost, IMU-based real-time on device gesture recognition glove. In *2020 IEEE International Conference on Systems, Man, and Cybernetics (SMC)*. IEEE, 3346–3351.
- [49] Charles Malleson, John Collomosse, and Adrian Hilton. 2020. Real-time multi-person motion capture from multi-view video and IMUs. *International Journal of Computer Vision* 128 (2020), 1594–1611.
- [50] Charles Malleson, Andrew Gilbert, Matthew Trumble, John Collomosse, Adrian Hilton, and Marco Volino. 2017. Real-time full-body motion capture from video and imus. In *2017 International Conference on 3D Vision (3DV)*. IEEE, 449–457.
- [51] Jennifer L McGinley, Richard Baker, Rory Wolfe, and Meg E Morris. 2009. The reliability of three-dimensional kinematic gait measurements: a systematic review. *Gait & posture* 29, 3 (2009), 360–369.
- [52] Salvador Medina, Denis Tome, Carsten Stoll, Mark Tiede, Kevin Munhall, Alexander G. Hauptmann, and Iain Matthews. 2022. Speech Driven Tongue Animation. In *Proceedings of the IEEE/CVF Conference on Computer Vision and Pattern Recognition (CVPR)*. 20406–20416.
- [53] Vladimir Medved. 2021. *Measurement and Analysis of Human Locomotion*. Springer.
- [54] Brice Michoud, Erwan Guillou, Hector Briceno, and Saïda Bouakaz. 2007. Real-time marker-free motion capture from multiple cameras. In *2007 IEEE 11th International Conference on Computer Vision*. IEEE, 1–7.
- [55] Emily Miller, Kenton Kaufman, Trevor Kingsbury, Erik Wolf, Jason Wilken, and Marilynn Wyatt. 2016. Mechanical testing for three-dimensional motion analysis reliability. *Gait & posture* 50 (2016), 116–119.
- [56] Chaithanya Kumar Mummadi, Frederic Philips Peter Leo, Keshav Deep Verma, Shivaji Kasireddy, Philipp M Scholl, Jochen Kempfle, and Kristof Van Laerhoven. 2018. Real-time and embedded detection of hand gestures with an IMU-based glove. In *Informatics*, Vol. 5. MDPI, 28.
- [57] Noitom 2015. Noitom Motion Capture Systems. <https://www.noitom.com/>.
- [58] Kyle Olszewski, Joseph J Lim, Shunsuke Saito, and Hao Li. 2016. High-fidelity facial and speech animation for VR HMDs. *ACM Transactions on Graphics (TOG)* 35, 6 (2016), 1–14.
- [59] Pascal Paysan, Reinhard Knothe, Brian Amberg, Sami Romdhani, and Thomas Vetter. 2009. A 3D face model for pose and illumination invariant face recognition. In *2009 sixth IEEE international conference on advanced video and signal based surveillance*. Ieee, 296–301.
- [60] Gerard Pons-Moll, Andreas Baak, Juergen Gall, Laura Leal-Taixe, Meinard Mueller, Hans-Peter Seidel, and Bodo Rosenhahn. 2011. Outdoor human motion capture using inverse kinematics and von mises-fisher sampling. In *2011 International Conference on Computer Vision*. IEEE, 1243–1250.
- [61] Gerard Pons-Moll, Andreas Baak, Thomas Helten, Meinard Müller, Hans-Peter Seidel, and Bodo Rosenhahn. 2010. Multisensor-fusion for 3d full-body human motion capture. In *2010 IEEE Computer Society Conference on Computer Vision and Pattern Recognition*. IEEE, 663–670.
- [62] Ammar Qammar and Antonis A Argyros. 2023. A Unified Approach for Occlusion Tolerant 3D Facial Pose Capture and Gaze Estimation using Mocap-NETs. In *Proceedings of the IEEE/CVF International Conference on Computer Vision*. 3178–3188.
- [63] QST Inc. 2012. QST Corporation Limited. <https://www.qstcorp.com/>.
- [64] Clément Reverdy, Sylvie Gibet, and Caroline Larboulette. 2015. Optimal marker set for motion capture of dynamical facial expressions. In *Proceedings of the 8th ACM SIGGRAPH Conference on Motion in Games*. 31–36.
- [65] Qaiser Riaz, Guanhong Tao, Björn Krüger, and Andreas Weber. 2015. Motion reconstruction using very few accelerometers and ground contacts. *Graphical Models* 79 (2015), 23–38.
- [66] Daniel Roetenberg, Henk J Luinge, Chris TM Baten, and Peter H Veltink. 2005. Compensation of magnetic disturbances improves inertial and magnetic sensing of human body segment orientation. *IEEE Transactions on neural systems and rehabilitation engineering* 13, 3 (2005), 395–405.
- [67] Javier Romero, Dimitrios Tzionas, and Michael J Black. 2017. Embodied hands. *ACM Transactions on Graphics* 36, 6 (2017), 1–17.

- [68] Martin Schepers, Matteo Giuberti, Giovanni Bellusci, et al. 2018. Xsens MVN: Consistent tracking of human motion using inertial sensing. *Xsens Technol* 1, 8 (2018), 1–8.
- [69] Soshi Shimada, Vladislav Golyanik, Patrick Pérez, and Christian Theobalt. 2023. Decaf: Monocular Deformation Capture for Face and Hand Interactions. arXiv:2309.16670 [cs.CV]
- [70] Ronit Slyper and Jessica K Hodgins. 2008. Action capture with accelerometers. In *Proceedings of the 2008 ACM SIGGRAPH/Eurographics symposium on computer animation*. 193–199.
- [71] William AP Smith, Alassane Seck, Hannah Dee, Bernard Tiddeman, Joshua B Tenenbaum, and Bernhard Egger. 2020. A morphable face albedo model. In *Proceedings of the IEEE/CVF Conference on Computer Vision and Pattern Recognition*. 5011–5020.
- [72] SONY 2023. Mobile Motion Capture "mocopi". <https://www.sony.net/Products/mocopi-dev/en/>.
- [73] Jochen Tautges, Arno Zinke, Björn Krüger, Jan Baumann, Andreas Weber, Thomas Helten, Meinard Müller, Hans-Peter Seidel, and Bernd Eberhardt. 2011. Motion reconstruction using sparse accelerometer data. *ACM Transactions on Graphics (ToG)* 30, 3 (2011), 1–12.
- [74] Anh Tuan Tran, Tal Hassner, Iacopo Masi, and Gérard Medioni. 2017. Regressing robust and discriminative 3D morphable models with a very deep neural network. In *Proceedings of the IEEE conference on computer vision and pattern recognition*. 5163–5172.
- [75] Zarins Uldis. 2017. *Anatomy of Facial Expressions*. Anatomy Next, Inc.
- [76] UnrealEngine. 2023. Live Link Face. <https://apps.apple.com/us/app/live-link-face/id1495370836>.
- [77] Rachel V Vitali, Ryan S McGinnis, and Noel C Perkins. 2020. Robust error-state Kalman filter for estimating IMU orientation. *IEEE Sensors Journal* 21, 3 (2020), 3561–3569.
- [78] Daniel Vlasic, Rolf Adelsberger, Giovanni Vannucci, John Barnwell, Markus Gross, Wojciech Matusik, and Jovan Popović. 2007. Practical motion capture in everyday surroundings. *ACM transactions on graphics (TOG)* 26, 3 (2007), 35–es.
- [79] Daniel Vlasic, Ilya Baran, Wojciech Matusik, and Jovan Popović. 2008. Articulated mesh animation from multi-view silhouettes. In *Acm Siggraph 2008 papers*. 1–9.
- [80] Timo Von Marcard, Roberto Henschel, Michael J Black, Bodo Rosenhahn, and Gerard Pons-Moll. 2018. Recovering accurate 3d human pose in the wild using imus and a moving camera. In *Proceedings of the European conference on computer vision (ECCV)*. 601–617.
- [81] Timo Von Marcard, Gerard Pons-Moll, and Bodo Rosenhahn. 2016. Human pose estimation from video and imus. *IEEE transactions on pattern analysis and machine intelligence* 38, 8 (2016), 1533–1547.
- [82] Timo Von Marcard, Bodo Rosenhahn, Michael J Black, and Gerard Pons-Moll. 2017. Sparse inertial poser: Automatic 3d human pose estimation from sparse imus. In *Computer graphics forum*, Vol. 36. Wiley Online Library, 349–360.
- [83] Thibaut Weise, Sofien Bouaziz, Hao Li, and Mark Pauly. 2011. Realtime performance-based facial animation. *ACM transactions on graphics (TOG)* 30, 4 (2011), 1–10.
- [84] Alexander Winkler, Jungdam Won, and Yuting Ye. 2022. QuestSim: Human motion tracking from sparse sensors with simulated avatars. In *SIGGRAPH Asia 2022 Conference Papers*. 1–8.
- [85] Dongseok Yang, Doyeon Kim, and Sung-Hee Lee. 2021. Lobstr: Real-time lower-body pose prediction from sparse upper-body tracking signals. In *Computer Graphics Forum*, Vol. 40. Wiley Online Library, 265–275.
- [86] Xinyu Yi, Yuxiao Zhou, and Feng Xu. 2021. Transpose: Real-time 3d human translation and pose estimation with six inertial sensors. *ACM Transactions on Graphics (TOG)* 40, 4 (2021), 1–13.
- [87] Jae Shin Yoon, Takaaki Shiratori, Shoou-I Yu, and Hyun Soo Park. 2019. Self-supervised adaptation of high-fidelity face models for monocular performance tracking. In *Proceedings of the IEEE/CVF Conference on Computer Vision and Pattern Recognition*. 4601–4609.
- [88] Jun Yu and Zengfu Wang. 2017. A video-based facial motion tracking and expression recognition system. *Multimedia Tools and Applications* 76 (2017), 14653–14672.
- [89] Qilong Yuan and I-Ming Chen. 2014. Localization and velocity tracking of human via 3 IMU sensors. *Sensors and Actuators A: Physical* 212 (2014), 25–33.
- [90] Longwen Zhang, Qiwei Qiu, Hongyang Lin, Qixuan Zhang, Cheng Shi, Wei Yang, Ye Shi, Sibe Yang, Lan Xu, and Jingyi Yu. 2023. DreamFace: Progressive Generation of Animatable 3D Faces under Text Guidance. arXiv:2304.03117 [cs.GR]
- [91] Li Zhang, Noah Snavely, Brian Curless, and Steven M Seitz. 2004. Spacetime faces: high resolution capture for modeling and animation. In *ACM SIGGRAPH 2004 Papers*. 548–558.
- [92] Longwen Zhang, Chuxiao Zeng, Qixuan Zhang, Hongyang Lin, Ruixiang Cao, Wei Yang, Lan

- Xu, and Jingyi Yu. 2022. Video-driven Neural Physically-based Facial Asset for Production. arXiv:2202.05592 [cs.CV]
- [93] Zhengyou Zhang. 2012. Microsoft kinect sensor and its effect. *IEEE multimedia* 19, 2 (2012), 4–10.
- [94] Zhe Zhang, Chunyu Wang, Wenhui Qin, and Wenjun Zeng. 2020. Fusing wearable imus with multi-view images for human pose estimation: A geometric approach. In *Proceedings of the IEEE/CVF Conference on Computer Vision and Pattern Recognition*. 2200–2209.
- [95] Zerong Zheng, Tao Yu, Hao Li, Kaiwen Guo, Qionghai Dai, Lu Fang, and Yebin Liu. 2018. Hybridfusion: Real-time performance capture using a single depth sensor and sparse imus. In *Proceedings of the European Conference on Computer Vision (ECCV)*. 384–400.
- [96] Yi Zhou, Wei Zhang, Xiaoou Tang, and Harry Shum. 2005. A bayesian mixture model for multi-view face alignment. In *2005 IEEE Computer Society Conference on Computer Vision and Pattern Recognition (CVPR'05)*, Vol. 2. IEEE, 741–746.
- [97] Xiangyu Zhu, Xiaoming Liu, Zhen Lei, and Stan Z Li. 2017. Face alignment in full pose range: A 3d total solution. *IEEE transactions on pattern analysis and machine intelligence* 41, 1 (2017), 78–92.